Research Article Open Access

Salimeh Kimiagar and Fahimeh Abrinaei*

Effect of temperature on the structural, linear, and nonlinear optical properties of MgO-doped graphene oxide nanocomposites

DOI 10.1515/nanoph-2017-0030
Received February 23, 2017; revised May 18, 2017; accepted May 19, 2017

Abstract: Magnesium oxide (MgO)-graphene oxide (GO) nanocomposites were prepared by the hydrothermal method at different temperatures. The effect of growth temperature on the structural, linear, and nonlinear optical (NLO) parameters was investigated. The decoration of MgO on GO sheets was confirmed by X-ray diffraction, scanning electron microscopy, Fourier transform infrared, and UV-visible (UV-vis) spectroscopy analyses. The energy band-gaps of MgO-GO nanocomposites were calculated from UV-vis spectrum using Tauc plot. The NLO parameters of MgO-GO nanocomposites were calculated for the first time by the simple Z-scan technique with nanosecond Nd:YAG laser at 532 nm. The nonlinear absorption coefficient β and nonlinear refractive index n_2 for MgO-GO nanocomposites at the laser intensity of 1.1×10^8 W/cm^2 were measured to be in the order of 10^{-7} cm/W and 10^{-12} cm^2/W, respectively. The third-order NLO susceptibility of MgO-GO nanocomposites was measured in the order of 10^{-9} esu. The results showed that MgO-GO structures have negative nonlinearity as well as good nonlinear two-photon absorption at 532 nm. Furthermore, the NLO parameters increased by the enhancement of the growth temperature. As the investigation of new materials plays an important role in the advancement of optoelectronics, MgO-GO nanocomposites possess potential applications in NLO devices.

Keywords: MgO-GO nanocomposites; nonlinear optics; Z-scan technique.

1 Introduction

Many opportunities have been provided for nonlinear optical (NLO) devices by the rapid expansion of nanoscience and nanotechnology. A large number of nanomaterials have been shown to possess considerable NLO properties, which cultivate the design and construction of nanoscale optoelectronic and photonic devices [1, 2].

The nanocarbons from 3D carbon nanoparticles (graphite) to 0D fullerenes, to 1D carbon nanotubes (CNTs), and then to 2D graphene display significant NLO properties, which can be useful for optical applications. Graphene oxide (GO) comprises the 2D nanostructure of a combination of carbon and oxygen functional groups. GO possesses remarkable electronic, optical, and mechanical properties, and it is attractive for a wide range of technological applications. One possible route to exploit these functionalities is to use GO to create composite materials.

The synthesis of magnesium oxide (MgO)-GO nanocomposites with high-rate adsorption of methylene blue was reported by Heidarizad and Şengör, and they concluded that the high adsorption capacity of MgO-GO nanocomposites makes it a promising adsorbent for water and wastewater treatment [3]. The hydrogen adsorption of magnesium-doped GO was studied using the density functional theory calculations [4]. It has been found that hydroxyl can be reduced from the surface of GO by magnesium doping on the matter whether the hydroxyl exhibits an acidity or alkalinity.

Song et al. reported on the synthesis and NLO properties of reduced GO hybrid material covalently functionalized with zinc phthalocyanine (ZnPc) using the Z-scan technique at 532 nm with 4 ns laser pulses. They showed that RGO-ZnPc exhibits much larger NLO absorption coefficient and better optical limiting performance than those of individual GO, ZnPc, and GO-ZnPc hybrid. This is due to the combination of different NLO mechanisms containing the excited state absorption arising from numerous localized sp^2 carbon configurations, two-photon absorption (TPA) from the sp^3 domains, and saturable

***Corresponding author: Fahimeh Abrinaei,** Department of Physics, East Tehran Branch, Islamic Azad University, Tehran, Iran, e-mail: f.abrinaei@iauet.ac.ir
Salimeh Kimiagar: Nano Research Lab (NRL), Department of Physics, Central Tehran Branch, Islamic Azad University, Tehran, Iran

absorption (SA) from the sp^2 clusters in the RGO moiety, the reverse SA (RSA) originating from the ZnPc moiety, and the contribution of the efficient photo-induced electron transfer or energy transfer process between ZnPc and RGO [5].

Mansour et al. considered the NLO properties of carbon-black suspensions and discussed the limitations and optimization of carbon-black suspension-based optical limiters for nanosecond pulsed laser using the Z-scan technique [6]. Tutt and Boggess reviewed the NLO processes in various materials, such as fullerenes, organometallics, carbon-black suspensions, semiconductors, and liquid crystals, which can be used in passive optical limiting devices. Specifically, they considered the mechanisms of RSA, two-photon and free-carrier absorption, nonlinear refraction, and induced scattering of these materials. They reported that the fullerenes are RSA materials and may have application to optical limiting for the protection of eyes and sensor from harmful radiations [7]. Hasan et al. reviewed the fabrication, characterization, incorporation, and operation of SWNT-polymer and graphene-polymer composites as saturable absorbers for the generation of ultra-short laser pulses through passive mode locking. In their research, CNTs showed ultrafast second- and third-order nonlinearities and SA in the near-infrared (NIR) region [8]. In the other researches, graphene shows ultrafast carrier relaxation time and ultra-broadband resonate NLO response [9]. Some research findings have shown that graphene represents weak optical absorption due to high transparency essence and low band-gap energy and it is not arbitrary for NLO applications [10]. On the contrary, several works have reported on the NLO properties of GO and their results showed that this behavior is due to nonlinear scattering, TPA, and/or excited state absorption [11–13].

Up to now, few works have focused on the synthesis and investigation of optical, electrical, and thermal properties of MgO-GO. However, no work has yet been done on the NLO properties of MgO-GO. Here, we investigated the effect of temperature on the structural and NLO properties of MgO-GO nanocomposites. MgO-GO samples were synthesized using the hydrothermal method. Moreover, the morphological, structural, and linear optical properties of MgO-GO nanocomposites were also investigated using X-ray diffraction (XRD), Fourier transform infrared (FTIR), scanning electron microscopy (SEM), and UV-visible (UV-vis) spectroscopy. The nonlinear refractive index (n_2) and nonlinear absorption coefficient (β) of MgO-GO nanocomposites were calculated by the Z-scan technique and the effect of growth temperature was considered.

2 Materials and methods

2.1 Sample preparation

GO was synthesized using the process in Ref. [14]. In the first step, 15 mg GO was dissolved in 20 ml distilled water (1 h). Another solution was prepared by the dispersion of 5 mg MgO in 30 ml ethanol and continuously stirred for 2 h at 80°C. Then, the two solutions were mixed. The suspension was then transferred into 200 ml Teflon-lined stainless autoclave and heated at 150°C for 6 h. The reaction system was cooled down to room temperature naturally, which afforded well-crystallized MgO-GO. The resulting powders were washed several times with distilled water and then dried in an oven at 60°C overnight to obtain the final product. The sample was labeled as MgO-GO1. The same processes were repeated at 180°C and 210°C instead of 150°C, and these samples were tagged as MgO-GO2 and MgO-GO3, respectively.

2.2 Characterization

The structural properties of the MgO-GO sample were analyzed by a Philips X'Pert PRO Hola XRD with Cu Kα radiation with $\lambda = 1.5404$ Å. The absorption spectrum of the MgO-GO sample was investigated using a Perkin-Elmer UV-vis spectrometer between 200 and 800 nm. FTIR spectra were obtained with a Jasco FTIR-410 spectrophotometer from 500 to 4000 cm^{-1}. The SEM images of MgO-GO nanocomposites were acquired using a VEGA/TESCAN, XMU.

2.3 NLO characterization via the Z-scan setup

The schematic diagram of the Z-scan experimental setup for the measurement of the NLO parameters of MgO-GO samples is shown in Figure 1. The Z-scan technique is based on the spatial beam broadening and narrowing of the Gaussian beam in far field due to the presence of optical nonlinearity. A Q-switched Nd:YAG laser (Ekspla NL640 model, 532 nm, 10 ns, 200 Hz) was used as a light source. The sample was moved in the direction of light incidence near the focal spot of the lens. The radius of the beam waist ω_0 was calculated to be 37 μm at the focal point. The Rayleigh length $z_0 = \pi\omega_0^2/\lambda$ was estimated to be 8.08 mm, much greater than the thickness of the sample, which is an essential prerequisite for Z-scan experiments. The intensity

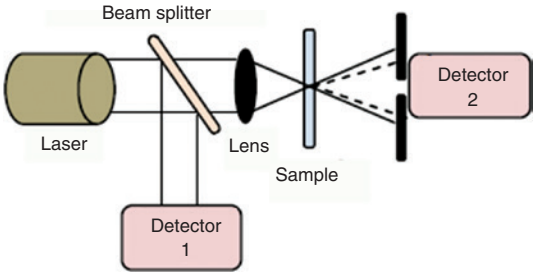

Figure 1: Z-scan experimental setup for the measurement of NLO parameters.

of the laser beam is 1.13×10^{8} W/cm^2 at the focal point. This setup was applied previously for the investigation of the NLO properties of $Mg(OH)_2$ nanostructures [15].

3 Results and discussion

3.1 Structural properties

Figure 2 shows the XRD spectra of GO, MgO and MgO-GO samples synthesized at various temperatures. As shown in Figure 2, in MgO-GO2 and MgO-GO3 samples, the exfoliation and reduction of GO are revealed by the complete absence of the peaks at $2\theta=10.01°$ and 8.79°, which are seen for GO and MgO-GO1 samples, respectively. A shift to low angle is observed for this peak in two mentioned samples. The partial shift of this peak and consequently increase in interlayer distance presumably is associated with the elimination of a few oxide groups of the GO.

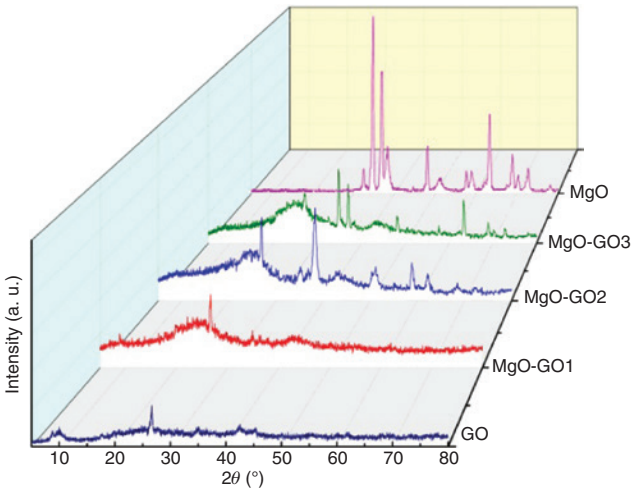

Figure 2: XRD spectra of GO, MgO, and MgO-GO samples.

A peak at $2\theta=26.6°$ is observed in all samples, which correspond to the characteristic peak of hexagonal pristine graphite and shift to the larger angles by adding MgO to GO as well as increasing the temperature.

After doping GO with MgO, a broad peak has been observed in all nanocomposites. This peak for the MgO-GO1 sample is started from $2\theta=12°$ to $2\theta=33°$. Also, the range of the wide peak is from $2\theta=14°$ to $2\theta=30°$ for the MgO-GO2 sample and from $2\theta=16.5°$ to $2\theta=29.5°$ for the MgO-GO3 sample. These peaks centered at $2\theta=24°$ for all three samples. The appearance of this broad peak at 24° indicates the restoration of van der Waals interaction between the carbon frameworks on the graphene sheets through reduction [16–19]. In addition, the appearance of these peaks in all samples after the addition of MgO announces the presence of the amorphous phase of MgO, with almost no crystalline structure. It is clear that the broadening of these peaks decreased by increasing the growth temperature. As the growth of MgO is related to growth temperature, by increasing the temperature, MgO peaks appear on the XRD pattern and the improvement of the crystalline phase can be seen.

For comparison, the XRD pattern of the MgO sample is plotted in Figure 2 as well. As can be seen from the XRD spectra, there is no clear peak for MgO in the MgO-GO1 sample synthesized at 150°C. By increasing the growth temperature to 180°C and 210°C, MgO-GO2 and MgO-GO3 nanocomposites clearly exhibit the peaks assigned to MgO. The sharper peaks in the MgO-GO3 sample than in the MgO-GO2 sample show that growth temperature is an important factor for the fabrication of MgO-GO nanocomposites.

To estimate the crystallite size of MgO-GO nanocomposites, the Hall-Williamson plot was used [20]. The crystallite size values of MgO-GO nanocomposites are listed in Table 1. In Table 1, the crystallite size of MgO-GO nanocomposites increased by increasing the growth temperature. Dreyer et al. showed that the functional groups such as carbonyl, hydroxyl, epoxide, and carboxyl at the GO surface may serve as nucleation sites that make possible the growth of nanomaterials on the GO surface [21]. By increasing the growth temperature, the peaks related to GO become weaker, and in return, the peaks attributed

Table 1: Grain size and band-gap values of GO and MgO-GO samples synthesized at different growth temperatures.

Samples	GO	MgO-GO1	MgO-GO2	MgO-GO3
Crystallite size (nm)	2.71	4.92	9.64	40.75
Band gap (eV)	3.3–4.2	2.6–3	4.2–5.9	4.6–6

to MgO becomes sharper; hence, the functional groups decreased as the temperature increased. Therefore, there are more nucleation sites for MgO in lower temperatures that lead to a smaller crystallite size [22].

3.2 Linear optical properties

The UV-vis spectra and Tauc plot of GO and MgO-GO samples are presented in Figure 3.

In Figure 3A (inset), the UV-vis spectrum of GO exhibited characteristic absorption bands with double absorption peaks: an intense absorption peak located at 230 nm and a weak one at 300 nm, which is marked by an arrow in Figure 3A (inset). The first peak is related to π-π* transition of the C=C bond and the latter one corresponds to n-π* transition of the C=O bonds of GO.

The UV-vis spectra and Tauc plot of MgO-GO1 sample are shown in the inset of Figure 3B. For the MgO-GO1 sample synthesized at 150°C, it can be seen that the weak peak located at 300 nm has disappeared as well as a red shift of the peak at 230 nm toward 265 nm due to the doping of GO with MgO. This red shift shows the reduction of GO and arises from the restoration of a π-conjugation network of reduced GO. In addition, the disappearance of the weak absorption peak at 300 nm vouches for the elimination of oxygen groups in reduced GO [23–25].

Figure 3C and D (inset) shows the UV-vis spectra and Tauc plot of the MgO-GO2 and MgO-GO3 sample produced by MgO doped-GO at 180°C and 210°C, respectively. These absorbance spectra exhibited a strong absorption in the region from 200 nm and decreased toward longer wavelengths. There is no trace of the absorption peak, which is observed in 265 nm for MgO-GO1, and it is vanished by increasing the growth temperature to 180°C as well as 210°C. As can be seen from the absorbance spectra, the peak is located at 230 nm for the MgO-GO1 sample that appeared as the shoulder for MgO-GO2 and MgO-GO3 samples marked by an arrow in Figure 3C and D (inset).

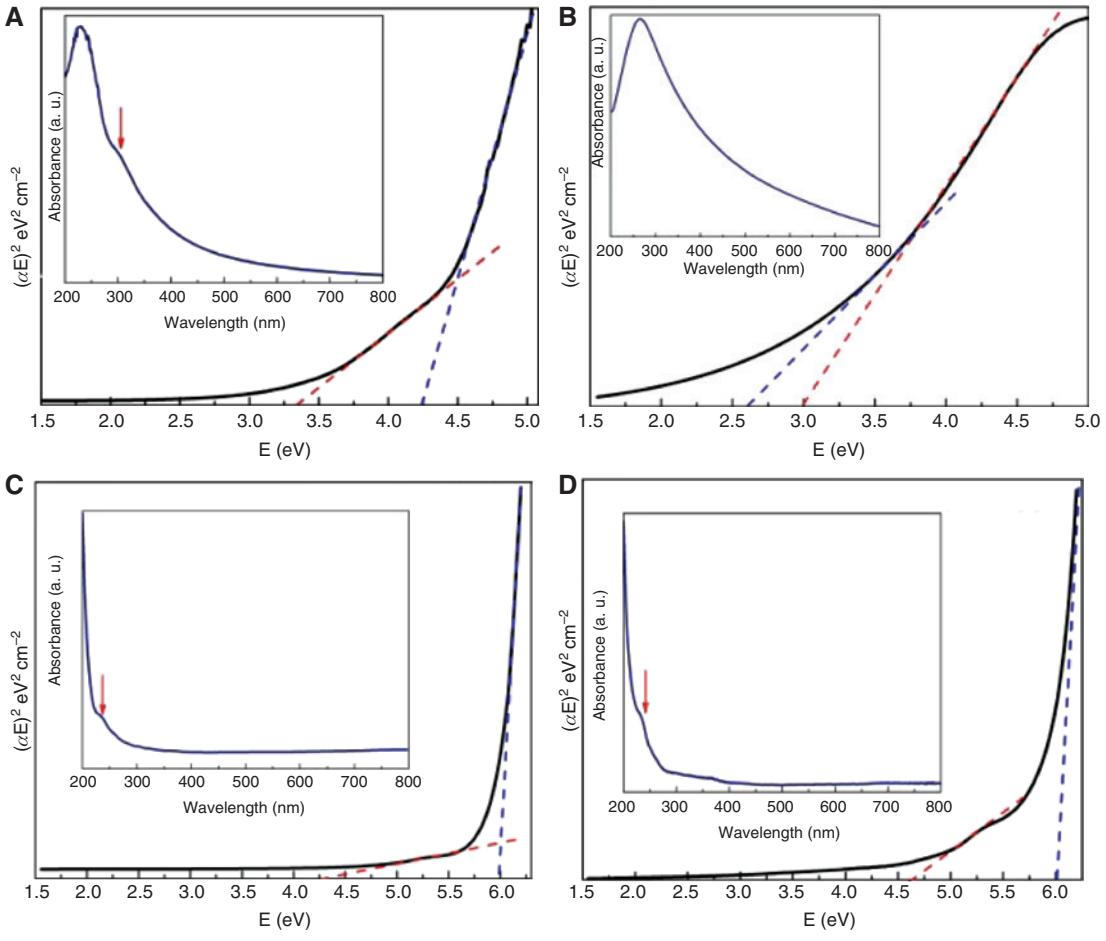

Figure 3: Tauc plot and absorbance spectra (inset) of GO and MgO-GO samples.
(A) GO, (B) MgO-GO1, (C) MgO-GO2, (D) MgO-GO3.

The absorption coefficient (α) of these samples can be calculated from UV-vis absorption data and use the formula of the Beer-Lambert law. α is used to calculate of band-gap energies, nonlinear absorption coefficients (β), and nonlinear refractive indices (n_2) of these samples.

From the UV-vis data, the optical band-gap values were calculated using the Tauc relation, $\alpha h\nu = A(h\nu - E_g)^n$, where α is the absorption coefficient, $h\nu$ is the energy (eV), E_g is the band-gap energy, and A is a constant. The parameter n is indicative of the nature of transition and for these samples is equal to ½.

The optical band-gaps of the four samples, GO and MgO-GO samples, were determined using a linear extrapolation to the Tauc plot as shown in Figure 3A–D. As the band-gap of GO is defined as a function of the oxidation degree or the contents of oxygen addends, it is not constant. Therefore, the amorphous GO sheet having a nonuniform oxidation level cannot exhibit sharp adsorption edges in the Tauc plot. Therefore, the optical band-gap of GO may be anywhere between semiconducting 1 eV and as high as 4.5 eV [26]. From the Tauc plot shown in Figure 3A for the GO sample, the optical band-gap value can be measured in the range of 3.3–4.2 eV, which has good agreement with the values reported for GO in the literature [27–29].

In Figure 3B, for the MgO-GO1 sample synthesized at 150°C, the Tauc plot exhibits sharp adsorption edge and a narrow range for the band-gap value is evaluated as 2.6–3 eV.

A range of band-gap, from 4.2 to 5.9 and from 4.6 to 6, was calculated for the MgO-GO2 and MgO-GO3 samples synthesized at 180°C and 210°C, respectively. This wide energy band-gap values may be due to the uneven oxidation of sheets. The optical band-gap values for all samples are listed in Table 1.

As can be understood from the XRD results, MgO in the MgO-GO1 sample has an amorphous structure, and by increasing the temperature to 180°C and 210°C for the MgO-GO2 and MgO-GO3 samples, the MgO structure is more and more crystallized. The XRD results confirm the calculated optical band-gap values from the Tauc plot drawing. With a complete crystallization process of MgO, the samples tend to semiconductor behavior and the band-gap values increase.

On the contrary, the calculated band-gaps of MgO-GO nanocomposites in all three samples are significantly smaller than the wide band-gap energy 7.8 eV expected for the bulk, pure, crystalline MgO. Therefore, it seems that MgO as a result of addition to GO can be close to metallic conduction behavior [30].

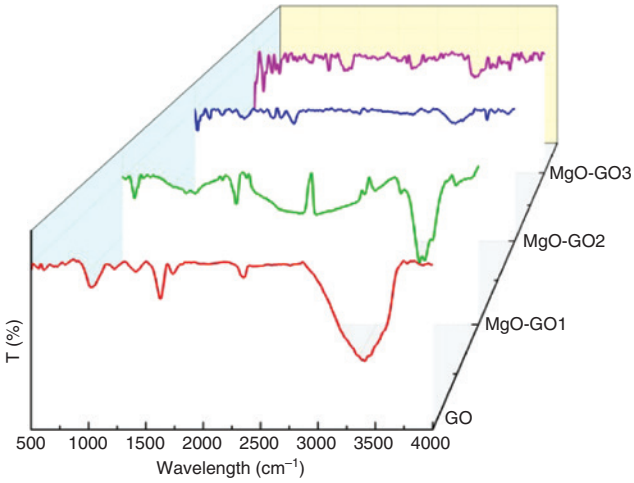

Figure 4: FTIR spectra of GO and MgO-GO samples.

The FTIR spectra for the GO and MgO-GO samples at different temperatures are shown in Figure 4. In Figure 4, several vibration frequencies are recorded in the GO sample, which indicates that the GO specimen has hydroxyl (-OH), carbonyl (-C=O), and epoxy (C-OC) groups. The spectrum of GO exhibits the presence of C-O (1050 cm^{-1}), O-H (1412 cm^{-1}), aromatic C=C (1640 cm^{-1}), and C=O (1726 cm^{-1}). The surface hydroxyl groups and water molecules with the main absorption band at 3400 cm^{-1} are assigned to the O-H group symmetry and asymmetry stretching vibrations [31]. This peak almost disappeared after increasing the growth temperature, suggesting a possible reduction of GO by MgO. For the MgO-GO samples by the growth temperature increasing to 210°C, the C-O absorption peak vanishes. The absorption band at 860 cm^{-1} contributed to the characteristic absorption peak of cubic MgO, which increases with temperature enhancement. It can be seen that the intense characteristic vibration of MgO exists in the band ranging from 500 to 1000 cm^{-1} with the absorption peak at 860 cm^{-1}, indicating the formation of cubic MgO [32]. The Mg-O stretching is observed below 700 cm^{-1} during the heat treating process with different temperatures at 180°C and 210°C [33].

3.3 Morphological analysis

To clarify the morphological properties of the synthesized MgO-GO materials, the SEM analysis was performed. The morphology of MgO-GO nanocomposites was elucidated from SEM images at lower and higher magnifications as shown in Figure 5.

A panoramic view of samples synthesized at three different temperatures demonstrates that all three

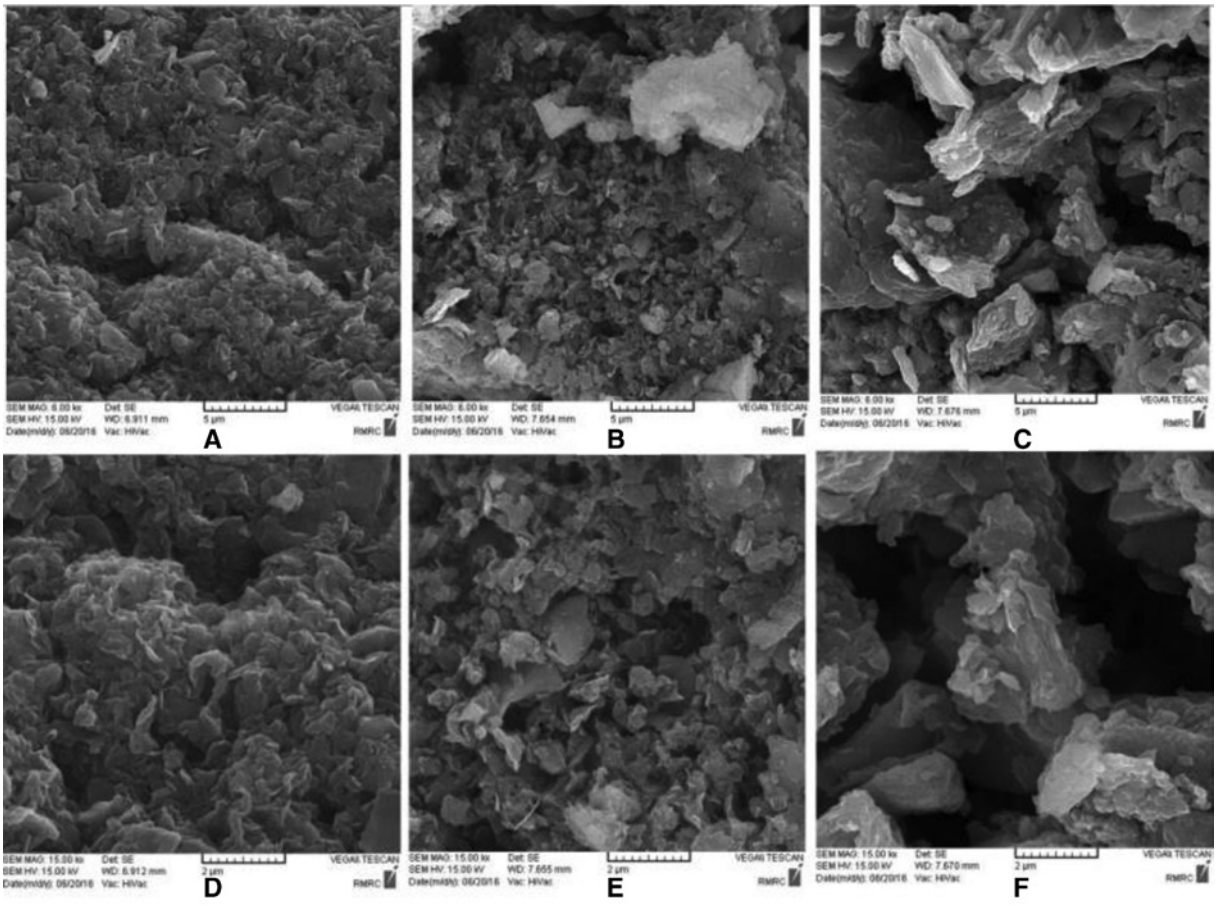

Figure 5: SEM images: MgO-GO1, MgO-GO2, and MgO-GO3 samples at (A–C) 6000× magnification and (D–F) at 15,000× magnification.

samples have a flake-like morphology, which confirms the removal of oxygen groups from the plane and the edges of reduced GO.

The SEM results indicate that the graphene sheets are exfoliated and decorated with MgO particles. Comparing the SEM images shows that, by increasing the growth temperature of MgO-GO samples, more MgO particles cover the surface of GO. The appearance of peaks corresponding to MgO in the XRD spectra with the increasing growth temperature confirms the SEM results. From the SEM images, it is clear that MgO particles are anchored nonuniformly on the surface of the reduced GO sheets.

3.4 NLO studies

The experimental setup for NLO measurements was shown in Figure 1 (Section 2). In the closed-aperture Z-scan experiment, the sample is transferred along the *z*-direction and the transmitted intensity is measured via an aperture in the far field. The normalized transmittance is plotted versus sample position *z*, which is measured with respect to the focal plane. From this curve, the sign of nonlinear refractive index n_2 consequently self-focusing or defocusing the quiddity of the sample can be determined. The magnitude of n_2 can be calculated from the closed-aperture curve as well as the following equations [34]:

$$\left|\Delta\varphi_0\right| = -\left(\frac{2\pi}{\lambda}\right) n_2 I_0 L_{\text{eff}} \tag{1}$$

where I_0 is the incident intensity at a focal point and L_{eff} is an effective sample thickness, which is calculated as

$$L_{\text{eff}} = \frac{1-e^{-\alpha L}}{\alpha} \tag{2}$$

where L is the actual thickness of the sample and the linear absorption α is measured from UV-vis data and the Beer-Lambert law for the MgO-GO samples. $|\Delta\varphi_0|$ in Eq. (1) is related to $\Delta\varphi_{p-v}$ as

$$\left|\Delta\varphi_{p-v}\right| = 0.406(1-S)^{0.25}\left|\Delta\varphi_0\right| \tag{3}$$

where $\Delta\varphi_{p-v}$ is the normalized difference between the peak and valley in the transmittance $T(z)$ and S is aperture's

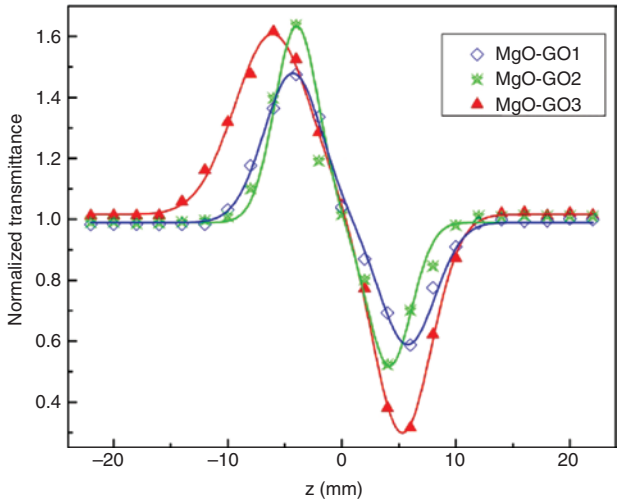

Figure 6: Closed-aperture of the Z-scan experimental curves of MgO-GO samples synthesized at various temperatures.

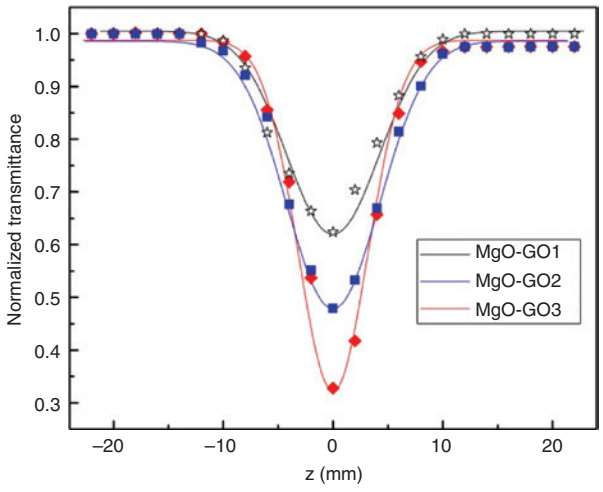

Figure 7: Open-aperture Z-scan data and fitting curves for MgO-GO nanocomposites.

Table 2: NLO parameters of GO-doped MgO samples.

Samples	MgO-GO1	MgO-GO2	MgO-GO3	Ref. [32]
L_{eff} (cm^{-1})	0.091	0.096	0.094	–
n_2 (cm^2/W)	-1.95×10^{-12}	-2.3×10^{-12}	-2.7×10^{-12}	$-O(10^{-12})$
β (cm/W)	9.7×10^{-8}	1.5×10^{-7}	1.8×10^{-7}	$O(10^{-7})$
Im χ^3 (esu)	1.7×10^{-9}	2.7×10^{-9}	3.2×10^{-9}	–
Re χ^3 (esu)	8.3×10^{-11}	9.8×10^{-11}	1.1×10^{-10}	–
$\lvert\chi^3\rvert$ (esu)	1.7×10^{-9}	2.7×10^{-9}	3.2×10^{-9}	$O(10^{-12})$

linear transmission, which is 0.3 for the closed-aperture Z-scan experiment in this work.

In Figure 6, the normalized transmittance is plotted as a function of the z-direction for MgO-GO nanocomposites synthesized at the different growth temperatures. In Figure 6, the sign of n_2 for all three samples is negative because the curves exhibited a valley after a peak. This situation demonstrates that all three samples act as self-defocusing materials [34].

Furthermore, the nonlinear refractive indices of the MgO-GO samples synthesized at 150°C, 180°C, and 210°C were obtained from the above equations in the order of the 10^{-12} cm^2/W, as listed in Table 2.

An open-aperture Z-scan experiment is carried out by the removal of the pinhole in Figure 1; thus, the transmitted beam arrives at the detector after passing the sample. The normalized transmittance is plotted versus the position of the sample (z). The presence of a peak or a valley in open aperture determined the NLO response of the sample to the light source. The magnitude of the nonlinear absorption coefficient β is calculated by fitting the experimental data to the following equation:

$$T(z)=\sum_{m=0}^{\infty}\frac{[-q_0(z,0)]^m}{(m+1)^{3/2}} \tag{4}$$

where $q_0(z,)=\beta I_0 L_{eff}/(1+z^2/z_0^2)$ and L_{eff}, β, I_0, and z_0 are the effective thickness sample, nonlinear absorption coefficient, laser intensity at the focal point, and diffraction length of the beam, respectively. The m parameter determines the order of the multiphoton processes; $m=1$ applies for TPA, $m=2$ for three-photon absorption (3PA), etc.

The open-aperture Z-scan curves are shown in Figure 7 for all the three MgO-GO samples. All the samples exhibit the transmittance with the minimum at $z=0$, which demonstrates RSA behavior for the MgO-GO samples synthesized at different temperatures. Using Eq. (4), the TPA curves are fitted to the experimental date that shows that the nonlinear absorption of these nanocomposites is predominantly due to the TPA mechanism. The solid curves in Figure 7 show the theoretical fitting of Eq. (4) to the experimental data. The nonlinear absorption coefficient is extracted by fitting the experimental data with Eq. (4) as a fitting parameter that is listed in Table 2 for easy comparison. The nonlinear absorption coefficient β of the MgO-GO1 sample prepared at 150°C is obtained in the order of 10^{-8} cm/W, whereas for two other samples it is found to be an order of magnitude larger than the β of the first sample and calculated in the order of 10^{-7} cm/W. Furthermore, the real and imaginary parts of χ^3 are listed in Table 2. The imaginary part of χ^3 is related to β as [34]

$$\mathrm{Im}\,\chi^3\ (\mathrm{esu})=(10^{-2}\,\varepsilon_0 c^2 n_0^2\lambda/4\pi^2)\beta\ (\mathrm{cm/W}) \tag{5}$$

The real part of χ^3 is related to n_2 as

$$\mathrm{Re}\,\chi^3\,(\mathrm{esu}) = (10^{-4}\varepsilon_0 c^2 n_0^2/\pi)n_2\ (\mathrm{cm}^2/\mathrm{W}) \quad (6)$$

where in Eq. (5) and Eq. (6), n_0 is refractive index, ε_0 is the vacuum permittivity, λ is the laser wavelength and c is the light velocity in vacuum.

In Table 2, the Im χ^3 is two orders of magnitude larger than the values for Re χ^3, which means that the absorption effect is stronger than the refraction for the MgO-GO samples. An increase in the NLO absorption can occur due to the increase of optical nonlinear interaction between the radiations and the particles. Therefore, an increase in crystallite size leads to an increase in the multiple scattering; thus, it increases the effective interaction length and consequently the nonlinear absorption is increased [35].

The third-order optical nonlinearities χ^3 are calculated using $\left|\chi^3\right| = \left[(\mathrm{Re}(\chi^3))^2 + (\mathrm{Im}(\chi^3))^2\right]^{1/2}$ equation for MgO-GO nanocomposites and are listed in Table 2.

In Table 2, the variations of growth temperature from 150°C to 210°C lead to an increase in β, n_2, and $|\chi^3|$ for MgO-GO nanocomposites.

To the best of our knowledge, there have been no reports of the investigation of the NLO properties of MgO-GO nanocomposites yet. Therefore, the comparison of the obtained results in this work with the same results was impossible. However, there are results for the NLO properties of other GO-based composites that show that the magnitude of the NLO parameters for MgO-GO nanocomposites is very satisfactory and that MgO-GO nanocomposites can be a promising candidate for NLO applications.

Biswas et al. studied the NLO properties of the GO-silver nanocomposite using the Z-scan technique via Q-switched Nd:YAG laser second harmonic radiation at 532 nm. They calculated β and n_2 in the order of 10^{-7} cm/W and 10^{-12} cm^2/W, respectively, which is in the same order of magnitude of β and n_2 in this work [36]. As silver and its composites have always been a good candidate for NLO applications, then the same order of magnitude for NLO parameters of MgO-GO and GO-Ag indicates that MgO-GO nanocomposites are a very promising candidate for NLO applications.

4 Conclusion

In this work, we have reported on the synthesis of MgO-GO nanocomposites by the simple hydrothermal method. The effect of growth temperature on the structural, linear, and NLO properties was investigated. XRD analysis, UV-vis spectroscopy, FTIR analysis, and SEM images confirmed the successful fabrication of MgO-GO nanocomposites.

The investigation of the NLO properties of MgO-GO nanocomposites under the excitation of nanosecond pulsed laser radiation at 532 nm wavelength is highlighted. The nonlinear absorption considerations show an increase in the TPA properties of MgO-GO nanocomposites with increasing growth temperature. The nonlinear absorption coefficients of MgO-GO nanocomposites are calculated in the order of 10^{-7} cm/W and they vary as much as an order of magnitude by an increase in growth temperature from 150°C to 180°C.

The closed-aperture Z-scan measurements show that the nonlinearity in MgO-GO samples is negative and the nonlinear refractive indices are in the order of 10^{-12} cm^2/W and increase with increasing growth temperature.

These results suggest that MgO-GO nanocomposites may be a very promising nonlinear medium and can be open an avenue to graphene-based nonlinear photonics.

References

[1] Loh KP, Bao QL, Eda G, Chhowalla M. Graphene oxide as a chemically tunable platform for optical applications. Nat Chem 2010;2:1015.
[2] Coleman JN, Lotya M, O'Neill A, et al. Two-dimensional nanosheets produced by liquid exfoliation of layered materials. Science 2011;331:568.
[3] Heidarizad M, Şengör SS. Synthesis of graphene oxide/magnesium oxide nanocomposites with high-rate adsorption of methylene blue. J Mol Liq 2016;224:607.
[4] Chen C, Zhang J, Zhang B, Duan HM. Hydrogen adsorption of Mg doped graphene oxide: a first principles study. J Phys Chem C 2013;117:4337.
[5] Song W, He C, Zhang W, et al. Synthesis and nonlinear optical properties of reduced graphene oxide hybrid material covalently functionalized with zinc phthalocyanine. Carbon 2014;77:1020.
[6] Mansour K, Soileau MJ, Van Stryland EW. Nonlinear optical properties of carbon-black suspensions (ink). J Opt Soc Am B 1992;9:1100.
[7] Tutt LW, Boggess TF. A review of optical limiting mechanisms and devices using organics, fullerenes, semiconductors and other materials. Prog Quant Electron 1993;17:299.
[8] Hasan T, Sun Z, Ferrari AC. Nanotube-polymer composites for ultrafast photonics. Adv Mater 2009;21:3874.
[9] Bonaccorso F, Sun Z, Hasan T, Ferrari AC. Graphene photonics and optoelectronics. Nat Photonics 2010;4:611.
[10] Wang HX, Wang Q, Zhou KG, Zhang HL. Graphene in light: design, synthesis and applications of photo-active graphene and graphene-like materials. Small 2013;9:1266.

[11] Liu Y, Zhou J, Zhang X, et al. Synthesis, characterization and optical limiting property of covalently oligothiophene-functionalized graphene material. Carbon 2009;47:3113.
[12] Wang AJ, Yu W, Huang Z, et al. Covalent functionalization of reduced graphene oxide with porphyrin by means of diazonium chemistry for nonlinear optical performance. Sci Rep 2016;6:23325.
[13] Liaros N, Aloukos P, Kolokithas-Ntoukas A, et al. Nonlinear optical properties and broadband optical power limiting action of graphene oxide colloids. J Phys Chem C 2013;117:6842.
[14] Kimiagar S, Rashidi N, Witkowski BS. Basic Blue 41 removal by microwave hydrothermal reactor reduced graphene oxide. Desalin Water Treat 2016;57:27269.
[15] Abrinaei F. Laser ablation of magnesium in water and investigation of optical nonlinearity by Z-scan technique. J Opt Soc Am B 2016;33:864.
[16] Liu P, Huang Y, Wang L. A facile synthesis of reduced graphene oxide with Zn powder under acidic condition. Mater Lett 2013;91:125.
[17] Wojtoniszak M, Chen X, Kalenczuk RJ, et al. Synthesis, dispersion, and cytocompatibility of graphene oxide and reduced graphene oxide. Colloids Surf B Biointerfaces 2012;89:79.
[18] Jin Y, Huang S, Zhang M, Jia M, Hu D. A green and efficient method to produce graphene for electrochemical capacitors from graphene oxide using sodium carbonate as a reducing agent. Appl Surf Sci 2013;268:541.
[19] Perera SD, Mariano RG, Nijem N, Chabal Y, Ferraris JP, Balkus KJ. Alkaline deoxygenated graphene oxide for supercapacitor applications: an effective green alternative for chemically reduced graphene. J Power Sources 2012;215:1.
[20] Rehani BR, Joshi PB, Lad KN, Pratap A. Crystallite size estimation of elemental and composite nano-powders using XRD principles. Indian J Pure Appl Phys 2006;44:157–61.
[21] Dreyer DR, Park S, Bielawski CW, Ruof RS. The chemistry of graphene oxide. Chem Soc Rev 2010;39:228–40.
[22] Kim S, Han KI, Lee IG, et al. A gallium oxide-graphene oxide hybrid composite for enhanced photocatalytic reaction. Nanomaterials 2016;6:127–32.
[23] Liu K, Zhang JJ, Cheng FF, Zheng TT, Wang C, Zhu JJ. Green and facile synthesis of highly biocompatible graphene nanosheets and its application for cellular imaging and drug delivery. J Mater Chem 2011;21:12034.
[24] Han Y, Luo Z, Yuwen L, Tian J, Zhu X, Wang L. Synthesis of silver nanoparticles on reduced graphene oxide under microwave irradiation with starch as an ideal reductant and stabilizer. Appl Surf Sci 2013;266:188.
[25] Zhou Y, Bao Q, Tang LAL, Zhong T, Loh KP. Hydrothermal dehydration for the "green" reduction of exfoliated graphene oxide to graphene and demonstration of tunable optical limiting properties. Chem Mater 2009;21:2950.
[26] Lim J, Rani JR, Choi K, Kim JH, Jun SC. Optical modification of atomic thickness graphene oxide. Int Soc Opt Photon. doi: 10.1117/2.1201210.004520.
[27] Kumar P, Bansiwal A, Labhsetwarb N, Jaina SL. Visible light assisted photocatalytic reduction of CO_2 using graphene oxide supported heteroleptic ruthenium complex. Green Chem 2015;17:1605.
[28] Ameer S, Gul IH, Mahmood N, Mujahid M. Synthesis, characterization and optical properties of in situ $ZnFe_2O_4$ functionalized rGO nano hybrids through modified solvothermal approach. Opt Mater 2015;45:69.
[29] Hsu H-C, Shown I, Wei HY, et al. Graphene oxide as a promising photocatalyst for CO_2 to methanol conversion. Nanoscale 2013;5:262.
[30] Kurth M, Graat PCJ, Mittemeijer EJ. The oxidation kinetics of magnesium at low temperatures and low oxygen partial pressures. Thin Solid Films 2006;500:61.
[31] Ezzatpour Ghadim E, Rashidi N, Kimiagar S, et al. Pulsed laser irradiation for environment friendly reduction of graphene oxide suspensions. Appl Surf Sci 2014;301:183.
[32] Pei LZ, Yin WY, Wang JF, Chen J, Fan CG, Zhang QF. Low temperature synthesis of magnesium oxide and spinel powders by a sol-gel process. Mater Res 2010;13:339.
[33] Fang Y, Wang R, Jiang G, et al. CuO/TiO_2 nanocrystals grown on graphene as visible-light responsive photocatalytic hybrid materials. Mater Sci B 2012;35:495.
[34] Sheik-Bahae M, Said AA, VanStryland EW. High-sensitivity, single-beam n_2 measurements. Opt Lett 1989;14:955–7.
[35] Sreeja R, Jobina J, Aneesh PM, Jayaraj MK. Linear and nonlinear optical properties of luminescent ZnO nanoparticles embedded in PMMA matrix. Opt Commun 2010;283:2908–13.
[36] Biswas S, Kole AK, Tiwary CS, Kumbhakar P. Enhanced nonlinear optical properties of silver-graphene oxide nanocomposite measured by Z-scan technique. RSC Adv 2016;6:10319.